

Electronic Supplementary Information

Spacer-controlled emission of randomly oriented fluorophores enhanced with surface plasmon-polaritons

Yu. Akimov^a and S. Sun^{a,b}*

^aElectronics and Photonics Department, Institute of High Performance Computing, Agency for Science, Technology and Research, 138632, Singapore.

^bMicrosystem & Terahertz Research Center, China Academy of Engineering Physics, No.596, Yinhe Road, Shuangliu, Chengdu, 610200, China.

*Corresponding author, Email: sunsong@mtrc.ac.cn

1. Computation of angular reflectance, SPP near-field enhancement, and power

The angular reflectance and SPP near-field enhancement, as well as the radiation and absorption powers of harmonic point dipoles with different orientations, were computed based on electromagnetic field calculation of plane waves in the multilayer structure shown in Figure 1 of the main text. The fields were calculated with the transfer-matrix method¹ for (i) p -polarized waves of λ_{ex} falling at angle θ from the substrate side for the fluorophore excitation study and (ii) for both s - and p -polarized waves of λ_{em} falling at angle θ from either the medium or substrate sides for the fluorophore emission study.

2. Excitation of SPP under the plane wave illumination

Fig. S1 shows the electric field enhancement across the Kretschmann configuration provided by excitation of SPPs at the incident wavelength $\lambda_{ex} = 633$ nm. For illustration, SiO₂ spacer with thickness $D_{sp} = 10$ nm and refractive index $n_{sp} = 1.52$ is used. The corresponding resonant angle is $\theta_{res} = 54.64^\circ$. The enhancement is normalized by the electric field intensity generated in unbounded water medium by a laser beam of the same power. Fig. S1 demonstrates field enhancement at the spacer/water interface provided by the excited SPP, which is used to enhance the excitation rate of the fluorophore there.

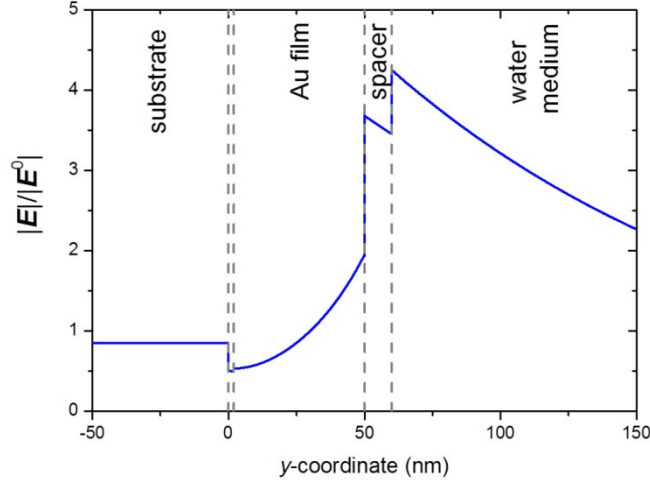


Fig. S1. Electric field enhancement across the Kretschmann configuration at the incident wavelength $\lambda_{ex} = 633$ nm with SiO₂ spacer of thickness $D_{sp} = 10$ nm and refractive index $n_{sp} = 1.52$. The highest field enhancement is observed at the spacer/water interface owing to the SPP excited in the gold film.

Fig. S2a shows the resonant reflectance $R_{res} = R(\theta_{res})$ as a function of spacer thickness D_{sp} for different spacer materials in the Kretschmann configuration for plane wave excitation at $\lambda_{ex} = 633$ nm. It demonstrates growth of the resonant reflectance with the spacer thickness D_{sp} , which causes the reduction of the total power P_{res} that goes into excitation of SPP, especially for high-index spacers. Fig. S2b shows the dependence of the effect power P_{res} normalized by the laser input power P_0 on spacer thickness D_{sp} . It demonstrates fast shrinking of P_{res} for thick spacers with high refractive index. It explains the decrease of excitation rate enhancement $\gamma_{ex}/\gamma_{ex}^0$ observed in Fig. 2d of the main text for higher-index spacers.

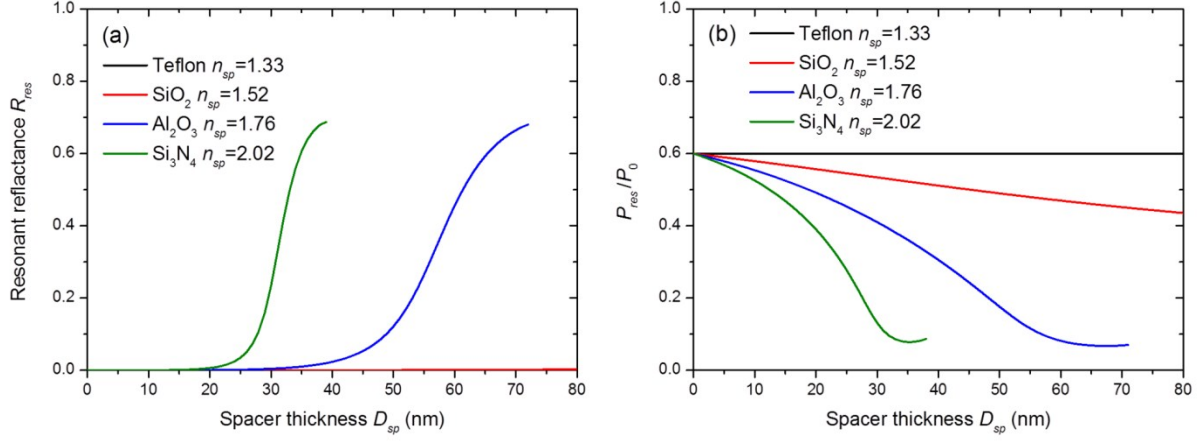


Fig. S2. (a) Resonant reflectance R_{res} of plane waves incident at $\lambda_{ex} = 633$ nm in the Kretschmann configuration. (b) Ratio of the total power P_{res} that goes into SPP excitation to the input power P_0 of the laser beam as a function of the spacer thickness D_{sp} .

3. Calculation of the radiative and total decay rate

For illustration, based on Eq. (7) in the main text, the corresponding enhancements on the radiative decay rates $\gamma_r(\theta_d, \phi_d)/\gamma_r^0 = P_r(\theta_d, \phi_d)/P_r^0$ are shown in Fig. S3 for the two classical dipole orientations: (a) perpendicular and (b) parallel with respect to the xz -plane. It demonstrates the enhancement of the dipole radiation provided in the Kretschmann configuration as a function of the spacer material and thickness. For small spacer thicknesses, radiation of the perpendicular dipoles prevails over that of the parallel dipoles, while for thicker spacers, radiation by the parallel dipoles becomes dominating.

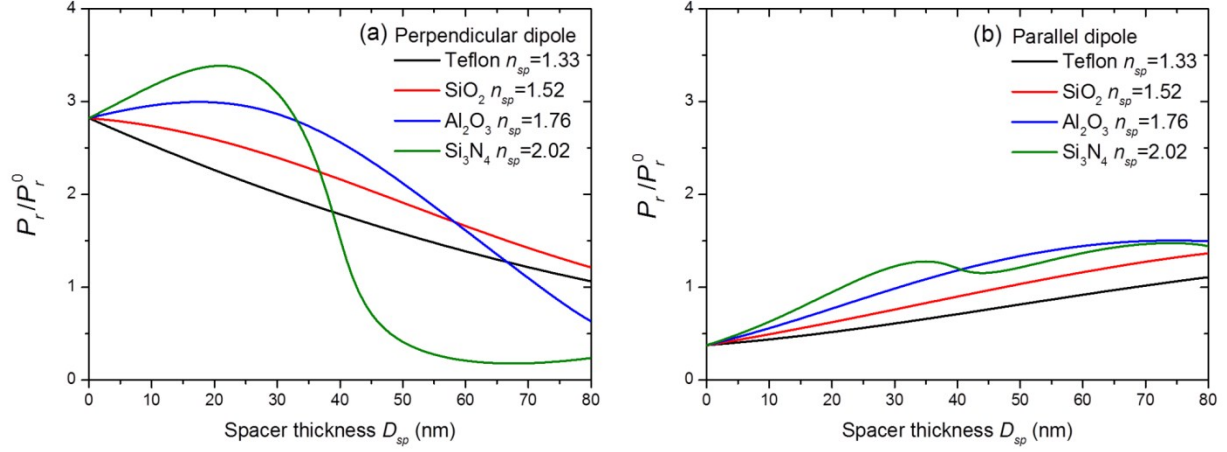


Fig. S3 Integrated power P_r radiated by the harmonic unit dipoles with (a) perpendicular and (b) parallel polarizations in the Kretschmann configuration with spacers of different thickness as compared to the total power P_r^0 radiated by a unit dipole in unbounded water medium.

Similarly, Fig. S4 shows the corresponding enhancements on the total decay rates from

$$\frac{\gamma_r(\theta_d, \phi_d) + \gamma_{abs}(\theta_d, \phi_d)}{\gamma_r^0} = \frac{P_r(\theta_d, \phi_d) + P_{abs}(\theta_d, \phi_d)}{P_r^0}$$

Eq. (9) in the main text for the (a) perpendicular and (b) parallel dipole orientations. It demonstrates the enhanced total decay rate of the harmonic dipole in the Kretschmann configuration provided by the high-index substrate and metal film.

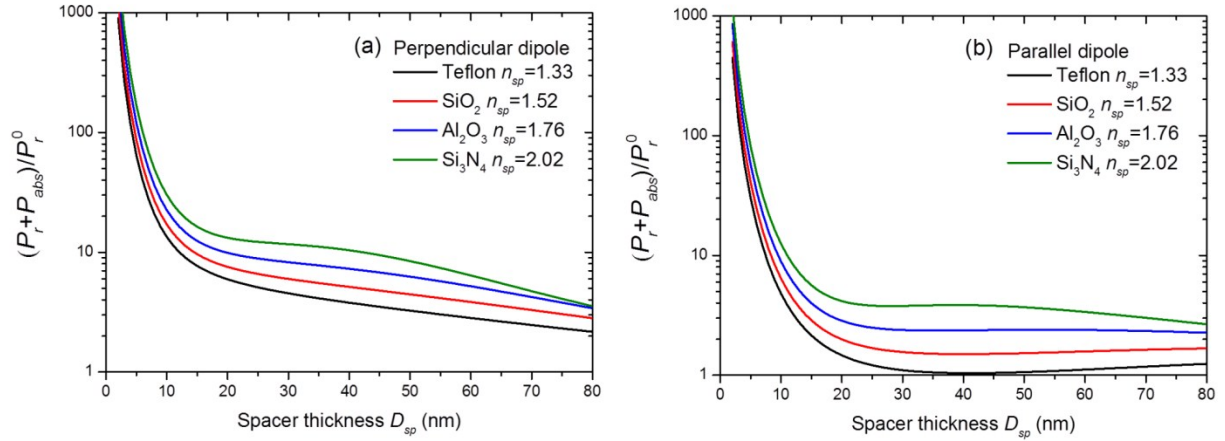


Fig. S4 Ratio of the overall emitted power $P_r + P_{abs}$ in the Kretschmann configuration to the power emitted in unbounded water medium P_r^0 as a function of the spacer thickness D_{sp} for the (a) perpendicular and (b) parallel harmonic dipoles. Fast growth of $P_r + P_{abs}$ at thinner spacers corresponds to the increased absorption in the metal film.

4. Quantum yields for perpendicular and parallel dipoles

The radiative decay rate [see Fig. S3] and the total emission rate of harmonic dipoles [see Fig. S4] were used to get the quantum yield enhancement, given by Eq. (3) of the main text. The corresponding enhancements are shown in Fig. S5 for the (a) perpendicular and (b) parallel dipole orientation. The obtained results demonstrate strong fluorescence quenching appearing for both orientations of the dipole momentum at thinner spacers with $D_{sp} < 2$ nm, whereby most of emitted photons decay non-radiatively due to the absorption by the metal film. As D_{sp} becomes thicker, the quantum yield grows as expected due to the giant suppression of the non-radiative decay component.

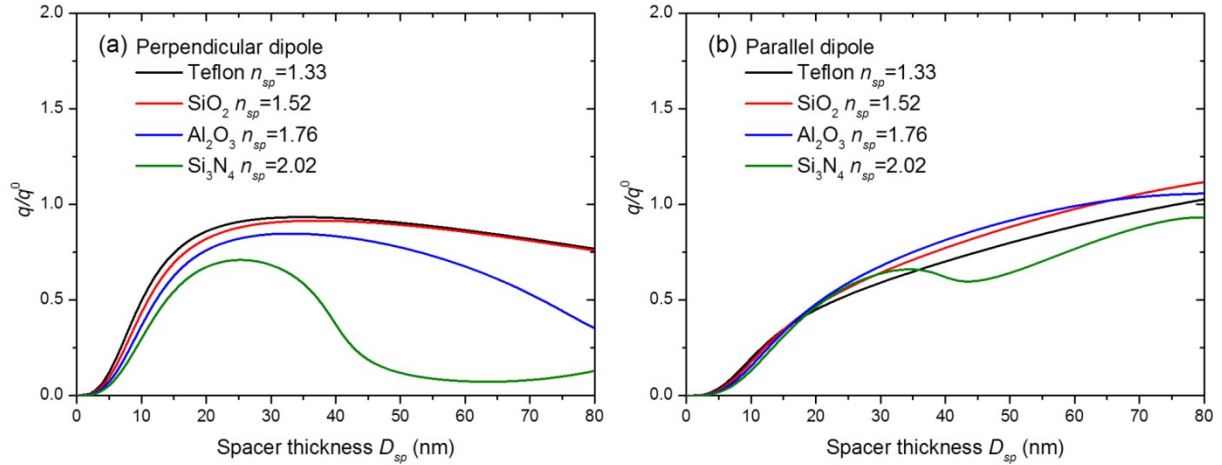


Fig. S5 Quantum yield enhancement provided by the Kretschmann configuration with different spacers for the (a) perpendicular and (b) parallel dipoles.

5. The average far-field radiation pattern of randomly oriented fluorophores for various spacer thicknesses

In complementary to Fig. 3b in the main text, Fig. S6a shows the average far-field radiation patterns for different thicknesses D_{sp} of Al_2O_3 spacers. The total power radiated towards the medium side demonstrates a monotonic growth with D_{sp} , while the total power radiated towards the substrate side exhibits a maximum with respect to spacer thickness. Note that in the case of $D_{sp} = 0$ nm, the fluorescence quenching is so strong that the unnormalized radiation pattern cannot be recognized. For comparison, Fig. S6b shows the average far-field radiation pattern of randomly oriented fluorophores in unbounded water medium, which is spherically symmetric as expected.

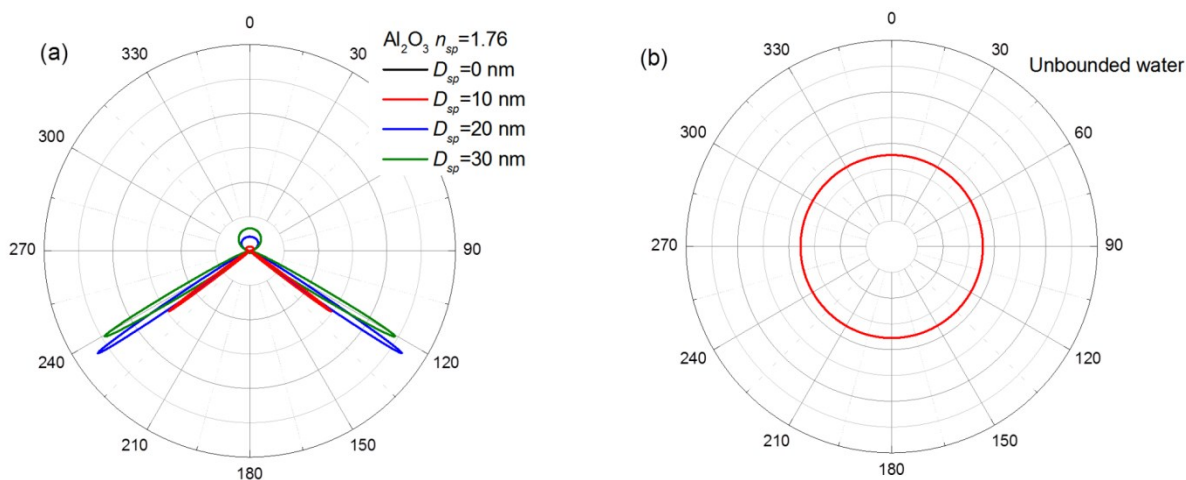


Fig. S6. Average far-field radiation patterns of fluorophores in (a) the Kretschmann configuration with Al_2O_3 spacers of different thicknesses and (b) in unbounded water medium. In the case of $D_{sp} = 0$ nm, the fluorescence quenching is so strong that the unnormalized radiation pattern cannot be recognized in the graph.

6. Far-field radiation pattern of dipoles with different orientations

Radiation patterns of the unit dipoles with three different orientations are demonstrated in Fig. S7a for the case of an Al_2O_3 spacer of 20 nm thickness. In all three cases, dipoles exhibit strong directional radiation towards the high index substrate regardless of the dipole orientation, because the original evanescent wave components in dipole emission in low index medium (e.g. water medium) transforms into propagating wave components in high refractive index medium (e.g. high index spacer and substrate). This result explains the highly directional radiation behavior in Fig. 3b in the main text. In contrast to the case of unbounded water as shown in Fig. S7b, the radiation is always symmetric with respect to the dipole polarization.

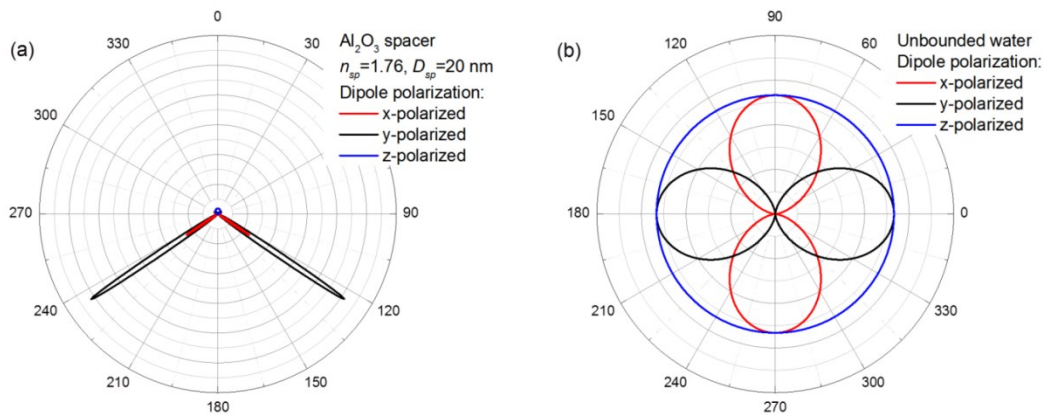


Fig. S7. Far-field radiation patterns of the harmonic unit dipoles with parallel and perpendicular polarizations in (a) the Kretschmann configuration with Al_2O_3 spacer of $D_{sp}=20$ nm and (b) in unbounded water medium.

References

1. Yu, Akimov. “Plasmonic properties of metal nanostructures” in *Plasmonic Nanoelectronics and Sensing*, edited by E. P. Li and H. S. Chu. Cambridge: Cambridge University Press, 2014, pp. 20-66.